Design and expected performance of a novel hybrid detector for very-high-energy gamma astrophysics

P. Assis[a,b], U. Barres de Almeida[c], A. Blanco[d], R. Conceição[a,b], B. D'Ettorre Piazzoli[e], A. De Angelis[f,g,b,a], M. Doro[h,f], P. Fonte[d], L. Lopes[d], G. Matthiae[i], M. Pimenta[b,a], R. Shellard[c], B. Tomé[a,b]

[a] *LIP Lisboa, Portugal*
[b] *IST Lisboa, Portugal*
[c] *CBPF, Rio de Janeiro, Brazil*
[d] *LIP Coimbra and University of Coimbra, Portugal*
[e] *Università di Napoli "Federico II" and INFN Roma Tor Vergata, Italy*
[f] *INFN Padova, Italy*
[g] *Università di Udine, Italy*
[h] *Università di Padova, Italy*
[i] *INFN and Università di Roma Tor Vergata, Roma, Italy*

arXiv:1607.03051v1 [astro-ph.IM] 11 Jul 2016

Abstract

Current detectors for Very-High-Energy γ-ray astrophysics are either pointing instruments with a small field of view (Cherenkov telescopes), or large field-of-view instruments with relatively large energy thresholds (extensive air shower detectors). In this article we propose a new hybrid extensive air shower detector sensitive in an energy region starting from about 100 GeV, allowing to detect with a 5σ significance a source as faint as 10% of the Crab Nebula in one year, and able to survey half of the sky. The instrument can detect a source with the luminosity of 25 Crab at 3σ in 1 minute, making it a very powerful tool to trigger observations of variable sources and to detect transients coupled to gravitational waves and gamma-ray bursts.

Keywords: Gamma-ray astronomy, Extensive air shower detectors, Transient sources, Gamma-ray bursts

1. Introduction

High energy gamma rays are important probes of extreme, non thermal, events taking place in the universe. Being neutral they can travel long distances without being deflected by galactic and extragalactic magnetic fields, hence allowing us to study directly their emission sources. The gamma emission is also related to the acceleration of charged cosmic rays and to the production of cosmic neutrinos. Gamma-rays can be, as well, the signature for the evidence of new physics at the fundamental scales, in particular by the annihilation or decay of new types of particles, as it is the case in many models. This motivation, associated to the advances of technology, has promoted a vigorous program of study of high energy gamma rays, with important scientific results (see [1, 2, 3, 4] for a summary of the main achievements).

The detected sources of cosmic gamma-rays above 30 MeV are concentrated around the disk of the Milky Way; in addition there is a set of extragalactic emitters. Roughly 3000 emitters above 30 MeV have been identified up to now, mostly by the Large Area Telescope (LAT) detector [5] onboard the *Fermi* satellite, and some 200 of them emit as well above 30 GeV [6] (see Fig. 1) - the region which is labeled the Very High Energy (VHE) region.

About half of the VHE gamma-ray emitters are objects in our Galaxy [7] and most of them can be associated to supernova remnants of various classes (shell supernova remnants, pulsar-wind nebulae, etc.). The remaining half are extragalactic. The angular resolution of present detectors – slightly better than 0.1° – is not good enough to assign the identified extragalactic emitters to any particular region in the host galaxies; however, there is some consensus that the signals detected from the Earth must be produced in the vicinity of supermassive black holes at the center of the galaxies [8].

Still, many problems remain open, of which we may mention:

- *The origin of cosmic rays* – it is well established that supernova remnants (SNRs) can accelerate protons up to few PeVs. However, the mechanism of acceleration of particles to energies of that order is still to be established experimentally. The study of the photon yield from Galactic sources for energies larger than 100 GeV and all the way up to PeV, might solve the problem (see for example [9]). Actually photons, which come from π^0 decay, correspond to hadronic cascades initiated at energies at least an order of magnitude larger.

- *The propagation of gamma-rays* – tells us about their interaction with the cosmic background radiation and is a

*Corresponding authors
Email addresses: ruben@lip.pt (R. Conceição), alessandro.deangelis@pd.infn.it (A. De Angelis), shellard@cbpf.br (R. Shellard)

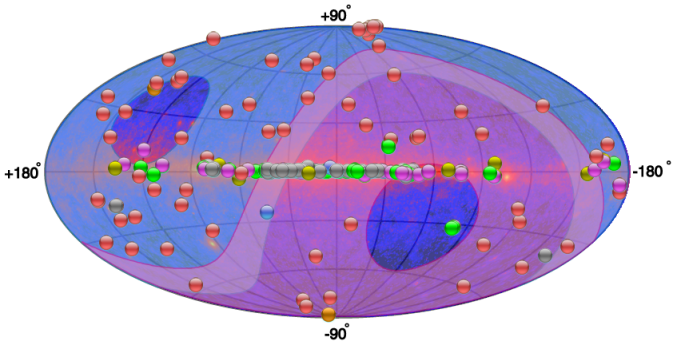

Figure 1: Sources of VHE emission plotted in galactic coordinates. The background represents the high-energy gamma-rays detected by *Fermi*-LAT. The clear blue (dominant on the left side) and pink (dominant on the right side) regions correspond respectively to the visible regions within 30° of the zenith from a detector approximately at the tropic in the Northern hemisphere and at the Southern hemisphere. From http://tevcat.uchicago.edu/, June 2016.

probe to cosmology themes.

- *New physics* – the ultimate nature of matter and of physics beyond the Standard Model, dark matter or new particles in general, the energy density of the vacuum or even quantum gravity may leave imprints in the spectrum of VHE gamma rays. High-energy gamma-ray astrophysics is sensitive to energy scales important for particle physics, in particular: the 100 GeV scale expected for cold dark matter; the TeV scale, where supersymmetric particles might appear; and finally, although indirectly, the unification scale and the Planck scale – an energy $\sim 10^{19}$ GeV, corresponding to a mass $\sqrt{\hbar c/G}$ (for discussion see for example [1] and references therein).

- *Transients* – Many VHE sources are characterized by variability, and it is important to be able to detect and measure the corresponding flares. Such flares have a duration that can go from few seconds – like for the short gamma-ray bursts or the expected counterparts of gravitational waves – to minutes for the long gamma-ray bursts, to minutes, hours or even days for the accretion flares of blazars (see e.g. [10] and references therein).

The layout of this paper is the following. In the Introduction we have briefly presented the field of very-high-energy gamma-ray astrophysics. In Section 2 we outline the characteristics of the existing detectors, and we explain why a large field-of view detector is needed. In Section 3 we make a case study with a possible design for such a detector. In Section 4 we describe the characteristics of the gamma-ray signal and of its background, and the various Monte Carlo samples used in the analysis of the performance of the new detector proposed. In Section 5 we evaluate the performance of such a new detector using the simulation. In Section 6 we analyze possible scenarios for such a detector, concentrating on the case study of the detection of VHE signals from transients. We conclude the paper with final remarks and a summary in Section 7.

2. Detection of gamma rays

The direct detection of primary X/γ-rays is only possible using satellite-based detectors: the radiation convert promptly in the atmosphere, whose thickness is about 28 radiation lengths at sea level. However, the cost of space technology limits the size of satellite-borne detectors to, roughly, areas of about one square meter. The largest and most sensitive space-based gamma detector is *Fermi*, with its high-energy subdetector, the LAT, with an area of about 3 m^2, and an effective area – the product of the geometrical area times the detection efficiency – of about 1 m^2 for a gamma-ray with an energy of 1 GeV [11].

If the energy of a primary cosmic photon is large enough (above some tens of GeV), part of the products of the shower generated by its interaction with the atmosphere, which acts as a calorimeter, can reach ground-based detectors. It is convenient to build such detectors at high altitudes, where atmospheric dimming is lower. The effective area of ground-based detectors can be much larger than the typical areas of satellites and since the fluxes of high-energy photons are low and decrease rapidly with increasing energy, TeV and PeV gammas can only be detected by ground-based detectors. Ground-based gamma-ray telescopes can detect the Cherenkov light emitted by atmospheric showers produced by primary photons and cosmic rays of energy much higher than those accessed by satellites.

The two kinds of detectors – on satellite and at ground – are complementary. The showers generated by photons at energies of the order of 1 GeV or so do not develop to a depth in the atmosphere sufficient to reach ground-based detectors, and thus the only way to detect photons below this energy is the use of satellites. At TeV energies, however, the flux is too low to be measured by satellite-based detectors – for areas of the order of one m^2 even the most luminous gamma source has a flux smaller than one photon per square meter every ten hours. Ground-based detectors have a large effective area, so their sensitivity is high, however they are subjected to a large amount of background events, typically charged cosmic rays. They outperform satellite-based detectors, like the *Fermi*-LAT, in the VHE energy region.

There are two main classes of ground-based VHE gamma detectors: the Extensive Air Shower (EAS) arrays and the Cherenkov telescopes.

2.1. EAS arrays

The EAS type of detectors, such as the High Altitude Water Cherenkov (HAWC) array [12, 13] which is presently in operation in Mexico, and the LHAASO detector [14] in China, for which construction is programmed to start soon, are large arrays of detectors sensitive to secondary particles, generated in the atmospheric showers. They have a high duty cycle and a large field-of-view, but a poor energy resolution. The energy threshold of such detectors is rather large, and they must be placed at altitudes of at least 4 km a.s.l., for a shower initiated by a 1 TeV photon has its maximum around 8 km a.s.l.

The principle of operation is the direct observation of the charged particles in the shower. This can be achieved:

- either by using a sparse array of scintillator-based detectors, as for example in the Tibet-AS [15] (for an energy of 100 TeV there are about 50 000 electrons in the shower at mountain-top altitudes), which has already finished operations;

- or by a dense coverage of the ground, to ensure efficient collection and hence lower the energy threshold. The ARGO-YBJ detector [16], an array of resistive plate chambers (RPC) at the Tibet site, followed this approach.

The energy threshold of EAS detectors is at best in the 0.5 TeV - 1 TeV range. At such energies fluxes are low and large surfaces of order of 10^4 m^2 at least are required.

The main problem in this class of detectors is the background rejection, for the flux of charged hadrons above 0.5 TeV is about a thousand times larger than that from the most intense gamma source, the Crab Nebula. Muon detectors are useful instruments to reduce background. Background rejection can be otherwise based on the reconstructed shower topology, which is different for gamma-initiated atmospheric showers and for hadron-initiated showers. The direction of the detected primary particles is computed from the arrival times with an angular precision which can reach about 1 degree at best. Energy resolution is poor.

The main EAS detector presently in operation is HAWC, a very high-energy gamma-ray observatory located in Mexico at an altitude of 4100 m. It consists of 300 steel tanks 7.3 m in diameter and 4.5 m deep, covering an instrumented area of about 22 000 m^2. Each tank is filled with purified water and contains four photomultipliers (PMT) of 20 cm diameter, which observe the Cherenkov light emitted by superluminal particles in water.

2.2. Cherenkov telescopes

Most of the experimental results on VHE photons are presently due to Imaging Atmospheric Cherenkov Telescopes (IACTs).

IACTs such as the third generation telescopes H.E.S.S., MAGIC and VERITAS detect the Cherenkov photons produced in air by charged, locally superluminal particles in atmospheric showers. For reasons explained below, they have a low duty cycle (about 1000 to 1500 hours per year) and a small field-of-view (FoV) of the order of $5^\circ \times 5^\circ$, but they have a high sensitivity and a low energy threshold (as low as 30 GeV for the present generation).

The observational technique used by the IACTs is to project the Cherenkov light collected in a large optical reflecting surface, of the order of 100-600 m^2, onto a camera in the focal plane of the reflector which is basically an array of photomultipliers, with typical quantum efficiency of about 30%; the camera has a typical diameter of about 1 m. The signal collected by the camera is transmitted to trigger systems, similar to the ones used in high-energy physics; the events which pass the trigger levels are sent to the data acquisition system, which operates at a frequency of a few hundreds Hz. The typical resolution on the arrival time of a signal on the focal camera is better than 1 ns - the shower has a duration of a few ns at ground.

About 10 photons per square meter arrive in a light pool of 100 m radius at 2000 m a.s.l. for a primary photon of 100 GeV; a light collector of area 100 m^2 is thus sufficient to detect gamma-ray showers. Due to the faintness of the signal, data can typically be taken only in moonless time or with moderate moonlight, and without clouds; this fact limits the total observation time and geographical places where they can be installed.

Showers induced by gamma-rays can be separated from the hadronic ones on the basis of the shower shape as recorded by the camera – the image is different for events produced by photons and by other particles; these characteristics can be used to reject the background from charged particles. The present identification techniques rely mostly on a strategy pioneered by Hillas in the 1980s [17]; the discriminating variables are called *Hillas parameters*. The intensity (and area) of the image produced provides an estimate of the shower energy, while the image orientation is related to the shower direction (photons "point" to emission sources, while hadrons are in first approximation isotropic).

Systems of more than one Cherenkov telescope provide a better background rejection, and a better angular and energy resolution, than a single telescope.

There are three large operating IACTs: the High Energy Stereoscopic System (H.E.S.S.) , the Major Atmospheric Gamma-ray Imaging Cherenkov Telescope (MAGIC), and the Very Energetic Radiation Imaging Telescope Array System (VERITAS), the former located in the southern hemisphere, and the two latter in the northern hemisphere. The typical sensitivities of H.E.S.S., MAGIC, VERITAS are such that a source as luminous as about 1% of Crab can be detected at a 5σ significance in 50 hours of observation for energies above 50-100 GeV.

A simplified comparison of the characteristics of the *Fermi* LAT satellite detector, of the IACTs and of the EAS detectors (ground-based), is given in Table 1.

3. Design of a novel detector

Either technique for ground-based observation of gamma-ray sources has clearly advantages and drawbacks. In this paper we shall propose a novel hybrid detector designed as a "dense" array for a surface of 10 000 m^2, that can solve some of the limitations of the present gamma-ray experiments, in the sense that:

- it can cover the energy range between 100 GeV and a few TeV, with a sensitivity large enough to detect possible transients;

- it has a wide field of view, being thus appropriate for increasing the chance to detect transients and monitor them over long baseline.

The detector we are going to propose can be the kernel for an EAS detector in which it is complemented by an external sparse detector array covering some 100 000 m^2 to increase the

Quantity	*Fermi*-**LAT**	**IACTs**	**EAS**
Energy range	20 MeV–200 GeV	100 GeV–50 TeV	400 GeV–100 TeV
Energy res.	5-10%	15-20%	$\sim$ 50%
Duty Cycle	80%	15%	$>$ 90%
FoV	$4\pi/5$	5 deg $\times$ 5 deg	$4\pi/6$
PSF	0.1 deg	0.07 deg	0.5 deg
Sensitivity	1% Crab (1 GeV)	1% Crab (0.5 TeV)	0.5 Crab (5 TeV)

Table 1: A comparison of the characteristics of *Fermi* LAT, of the present IACTs and of a typical EAS particle detector array. Sensitivity is computed over one year for *Fermi* and the EAS, and over 50 hours for the IACTs.

sensitivity above 5 TeV to make it comparable with the foreseen extension of HAWC and with the planned LHAASO detector.

ARGO and HAWC have both explored the concept of a single detector composed by: either a large carpet of RPCs with a very good time and space resolutions (ARGO), or a large set of Water Cherenkov Detectors WCD, each one with large volume of water (HAWC). The ARGO approach relies on a detailed knowledge of the charged particle pattern of the air showers at ground. The HAWC approach relies on the knowledge of the electromagnetic energy contents of the air shower integrated in one reasonable large size region at ground combined with a good discrimination power for single muons.

In this paper we argue that a hybrid concept composed by a carpet of low-cost RPCs on top of WCDs (or other Cherenkov detectors based on glass or lead glass) of reasonably small dimensions, benefits from the main advantages of both approaches and can reach a much better sensitivity at the lowest energies (around 100 GeV). This detector should be placed at high altitude (we assume 5200 m a.s.l. in this paper).

Our basic element used in this simulation, the station (Fig. 2), is constructed by putting together one WCD, with a rectangular horizontal surface of 3 m $\times$ 1.5 m and a depth of 0.5 m, with signals read by PMTs at both ends of the smallest vertical face of the block. On top of the WCD there are two RPCs, each with a surface of (1.5 $\times$ 1.5) m^2 and with 16 charge collecting pads. Each RPC is covered with a thin (5.6 mm) layer of lead, to provide secondary photon conversion: this can exploit the fact that these photons have a stronger correlation with the primary direction with respect to the secondary electrons of the shower.

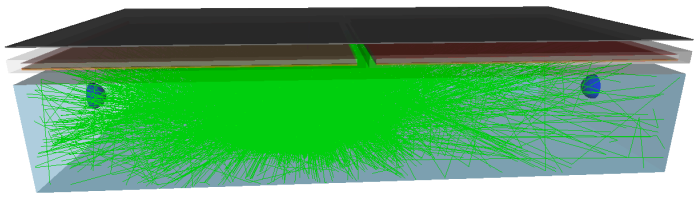

Figure 2: Basic detector station, with one WCD covered with RPCs and a thin slab of lead. The green lines show the tracks of the Cherenkov photons produced by the electron and positron from the conversion of a photon in the lead slab.

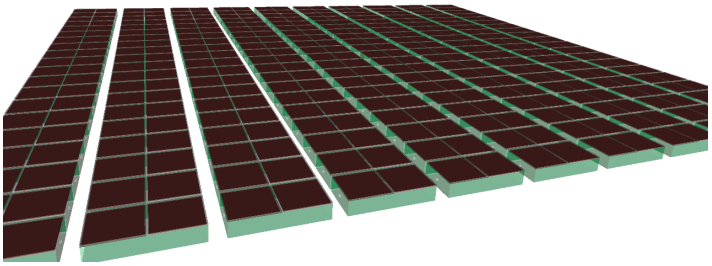

Figure 3: Layout of the detector used in the case study.

The full detector (Fig. 3) is deployed as an array of individual stations set in long lines with each touching the other on their largest dimension. The row of lines of detectors are separated by a small distance (roughly 0.5 m) to allow access to service the PMTs and the RPCs. This arrangement allows for a compact array and for a scaling of the full detector. The performance results presented herein are based on a baseline configuration with 60 rows and 30 lines, covering an effective area of about 10 000 m^2.

The proposed RPCs are of the MARTA type (see [18]) which have been developed in the last four years at LIP in Coimbra, Portugal, and successfully tested at Pierre Auger site in Malargüe, Argentina. These RPCs were designed to work at low gas flux, (1-4) cc/min, at harsh outdoor environment, and demanding very low maintenance services. Their intrinsic time resolution was measured to be better than 1 ns.

4. Signal, background and simulation tools

We have performed a Monte Carlo simulation of the detector to evaluate its performance.

For the simulation of atmospheric showers we use the CORSIKA (COsmic Ray SImulations for KAscade) (version 7.4100) program having the electromagnetic interaction been treated by the EGS4 routines [19]. The model to describe hadronic interactions is FLUKA [20, 21], together with the QGSJet-II [22] model for high-energy interactions.

Gamma and proton primaries are simulated both with fixed energies and with a power-law differential energy spectrum with index -1.0. Each shower is reprocessed 100 times, with

a new core position randomly set in each realization. Gamma rays are simulated as coming from a point-like source at a zenith angle of 10°, while protons are simulated with incoming directions spanning the range from 5° to 15° in zenith angle. In detail:

- Fixed energies: 10^4 showers were simulated in energy steps between 30 GeV and 100 GeV; for energies between 100 GeV and 1 TeV, 10^3 showers were produced. The maximum distance of the random core with respect to the center of the array is set according to the energy of the primary, varying between 200 m for $E_0 = 30$ GeV and 600 m for an initial energy $E_0 = 1$ TeV.
- Continuous energy spectrum: the minimum energy is 10 GeV for the photons and 40 GeV for the protons; the maximum energy is 5 TeV. About 2×10^3 showers were used for each primary, with the core generated inside an area of $(110 \times 110)\,\mathrm{m}^2$.

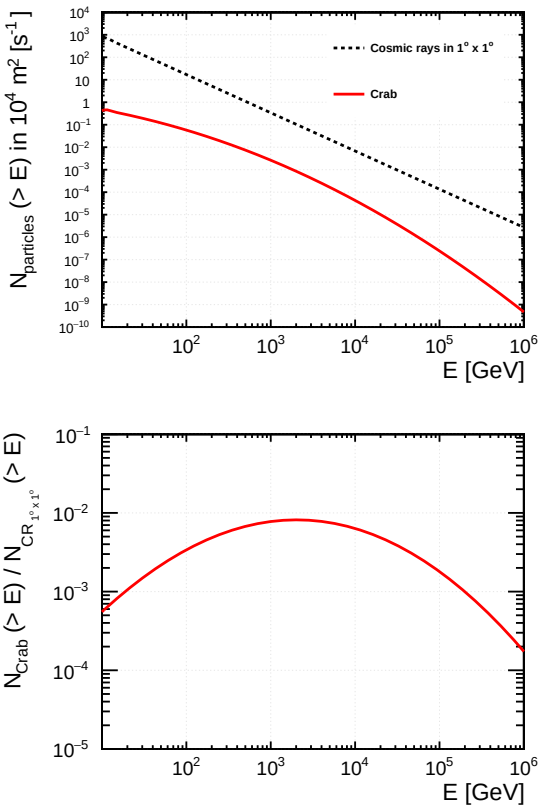

Figure 4: Top: Signal above a given energy on a surface of 10000 m^2, integrated over 1 second: Crab (solid line) and background from charged cosmic rays within one square degree (dashed line). Bottom: ratio signal/background from the above plot.

Once atmospheric showers have been simulated and the information of the electrons and photons reaching a height of 5200 m a.s.l. is recorded, we simulate the response of the detector stations using the GEANT4 [23, 24] toolkit.

In the baseline simulation of the WCD units, the photomultipliers have a diameter of 15 cm. The maximum quantum efficiency is 30% at $\lambda \sim 420$ nm. The inner walls of the tanks are covered with a white diffusive surface in order to increase the light collection. The specular and diffusive properties of this layer are accounted for, as well as its wavelength dependence. In more detail, the reflectivity was taken to be 95%, for $\lambda > 450$ nm, of which 80% is diffusively reflected and 20% is reflected according to a Gaussian angular distribution around the specular reflection direction, with a characteristic width of $\sigma_\alpha \sim 0.2°$. The detailed structure and materials of the RPC are also described in the simulation. In particular the information concerning the ionizing energy depositions in the gas is recorded for subsequent processing.

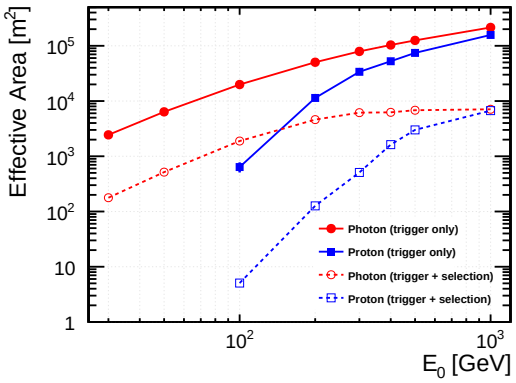

Figure 5: Effective area at trigger level (solid curves) and after the cuts used for the shower direction reconstruction (dashed curves), separately for gamma-ray- and proton-initiated showers.

The response of the tanks was studied for single vertical particles injected uniformly over the top surface. The mean number of photoelectrons for 20 MeV photons, the median energy at about 10 m from the shower core, is 15 p.e., while for relativistic muons it is 230 p.e.

In order to evaluate the performance of the detector, we consider a source with an emission energy distribution like the Crab Nebula.

The Crab Nebula is a nearby ($\sim$ 2 kpc away) pulsar wind nebula and the first source detected in VHE gamma-rays [25]. Moreover, it is the brightest steady VHE gamma-ray source, therefore it has become the so-called *standard candle* in VHE gamma-ray astronomy. Recent observation of flares in the GeV range [26, 27] have however shown that occasionally the Crab flux can vary.

The *stationary* flux from the Crab Nebula follows, according to the measurements from MAGIC [28], a law

$$\frac{dN_\gamma}{dE} \simeq 3.23{\times}10^{-11} \left(\frac{E}{\mathrm{TeV}}\right)^{-2.47-0.24\left(\frac{E}{\mathrm{TeV}}\right)} \mathrm{TeV}^{-1}\mathrm{s}^{-1}\mathrm{cm}^{-2}\,. \quad (1)$$

For the spectral energy distribution of background cosmic rays we have used the expression

$$\frac{dN}{dE} \simeq 1.8 \times 10^4 \left(\frac{E}{\mathrm{GeV}}\right)^{-2.7} \mathrm{GeV}^{-1}\mathrm{s}^{-1}\mathrm{sr}^{-1}\mathrm{m}^{-2}\,; \quad (2)$$

the approximation is valid from some 10 GeV to about 1 PeV.

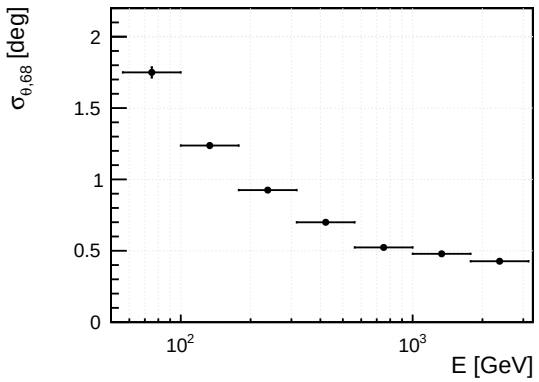

Figure 6: Angular resolution for gamma-ray primaries with zenith angle θ = 10°, as a function of the energy.

The number of photons from Crab per m^2 per second above a given threshold are shown in Fig. 4, and compared to the background from cosmic rays in a square degree.

The photon and proton showers, simulated with an energy spectrum with index -1.0, are weighted by $E_0 \times f(E_0)$, where f is the differential energy spectrum in Eqs. 1 and 2, respectively, and E_0 is the energy of the primary particle.

5. Estimated performance

5.1. Effective area at the trigger level

We use a trigger selection which requires that at least three stations have detected a signal; the trigger condition for each station requires at least 5 photoelectrons in either photomultiplier. Although a detailed study of trigger is out of the scope of this paper, a central trigger scheme with a few hardware and/or software stages can offer a good flexibility and be able to handle the expected trigger rates. The effective area at trigger level, i.e., the integral of the surface times the trigger efficiency, is shown in Fig. 5 for gamma-ray and proton initiated showers.

5.2. Angular resolution

We reconstruct the arrival direction of the particle initiating the shower from the positions and the arrival times of the hits in the RPC pads. The reconstruction is performed assuming a shower front plane model. It was considered a time resolution of σ_t = 1 ns, which can be achieved by present RPCs with standard electronics. In order to improve the angular reconstruction it is required that the event has at least 10 active RPC pads. The pad is only accepted for the reconstruction if it belongs to a triggered WCD stations. We compare the reconstructed angle with the angle in the simulation, and we calculate the 68% containment angle, $\sigma_{\theta,68}$. The results as a function of the reconstructed energy are shown in Fig. 6. A reasonable resolution, better than 2°, can be achieved at energies around 100 GeV.

5.3. Effective area at the reconstruction level

After the event selection for the shower direction reconstruction, we further require that the direction of gamma showers is within the 68% containment radius defined by the angular resolution. The effective area after these cuts is shown in Fig. 5, for proton-initiated showers and for gamma-initiated showers.

5.4. Energy estimate

The shower energy is reconstructed from the total signal, defined as the sum of the number of photoelectrons in all WCD stations. A calibration curve is obtained using the photon simulation with the Crab spectrum, by plotting the median of the generated photon energies in each bin of measured signal, as a function of the median of the measured signal. The dependence appears approximately linear for $E_0 > 300$ GeV.

The non-linearity, defined as the relative difference between the median of the reconstructed and true energies assuming the calibration constant computed for $E_0 > 300$ GeV, is shown in Fig. 7, top, as a function of the reconstructed energy.

The reconstructed energy follows quite well a log-normal distribution as a function of the generated energy. The energy resolution was thus calculated by fitting the distribution of $\ln(E/E_0)$ with a Gaussian function; the relative resolution is shown in Fig. 7, bottom. The resolution on the reconstructed photon energy depends both on the detector resolution and on the fluctuations in the shower development.

5.5. Hadron background suppression

The hybrid configuration of the detector units allows to combine the background rejection techniques used by ARGO and HAWC [13, 16]. Large signals in WCDs away from the core are mostly due to isolated muons, a characteristic signature of showers initiated by hadrons. In addition, the RPCs on top provide important additional information about the structure of isolated energetic particle clusters, which allows to further improve the gamma-hadron discrimination. The development of a hadron rejection algorithm, which combines the information of the two sub-dectectors is out of the scope of this article. Conservatively, no background rejection was considered below 200 GeV, and above this energy the performance of HAWC [29] was assumed.

5.6. Significance of the Crab signal

Gamma-initiated events have been selected within the angular window defined by the cone with half-aperture equal to the angular resolution for photons. The cosmic-ray background has been calculated for the same window, assuming an isotropic flux. The event rate in each bin of reconstructed energy, before background suppression, is shown in the top plot of Fig. 8.

We then computed the number of events for one year of effective time, after applying the hadron suppression efficiency curves; the result is shown separately for signal and background events in the bottom plot of Fig. 8. One year of effective time corresponds to 7.9×10^6 seconds, assuming a duty cycle of 25% (which corresponds to the average fraction of time at which a

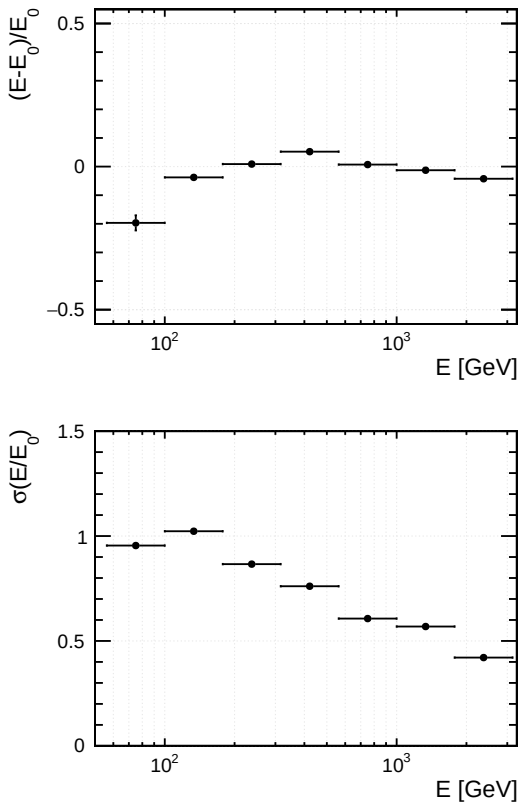

Figure 7: Top: Non-linearity in the reconstructed energy, for photons with a spectral energy distribution as for Crab nebula. Bottom: Resolution in the reconstructed energy, for the same sample of photon-initiated showers.

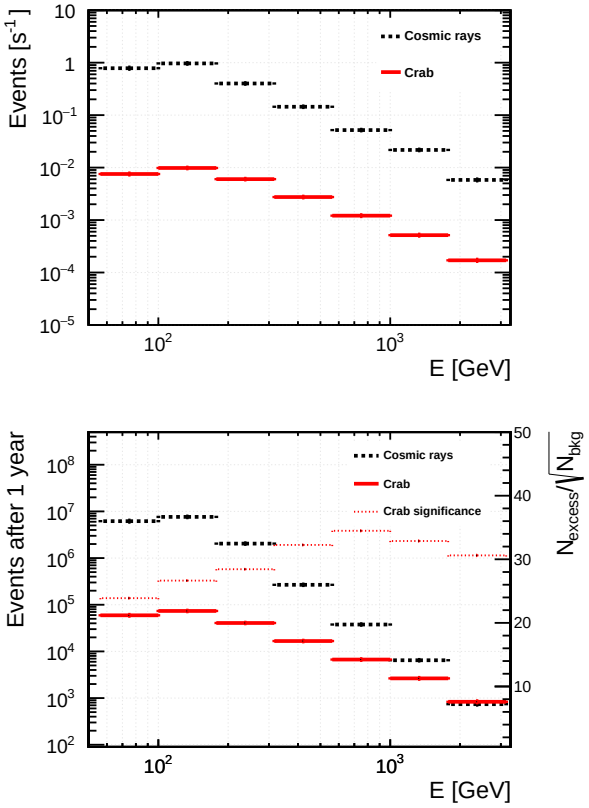

Figure 8: Top: Signal from Crab (solid line) and background from charged cosmic rays (dashed line) per second after the cuts in the 1σ angular region, before the background rejection. Bottom: Signal from Crab (solid line) and background (dashed line) in one year of effective time after all cuts. The Crab significance, expressed as the ratio between the signal and the square root of the background, is also shown.

source culminating at zenith is seen within an angle of 30° from zenith).

The significance of a detection in terms of number of standard deviations n_σ can be calculated with a simplified formula $n_\sigma \simeq N_{\rm excess}/\sqrt{N_{\rm bkg}}$, where $N_{\rm excess}$ is the number of excess events, and $N_{\rm bkg}$ is the background estimate, whenever $N_{\rm excess} \ll N_{\rm bkg}$. The significance of the Crab signal for one year is also shown in the bottom plot of Fig. 8.

5.7. Sensitivity for a steady source

To evaluate the performance of the detector, we compute its differential sensitivity, i.e. we investigate the sensitivity in narrow bins of energy (4 bins per decade). We compute the sensitivity as the flux of a source giving $N_{\rm excess}/\sqrt{N_{\rm bkg}} = 5$ after 1 year of effective observation time for a source visible for 1/4 of the time (this roughly corresponds to the visibility of the Galactic Centre from the Southern tropic).

The result is shown in Fig. 9, and compared with the one-year sensitivities of *Fermi* and HAWC.

The differential sensitivity is independent of the spectral energy distribution (SED) of the emitting source. To compute the total sensitivity one must assume a SED; from this assumption, one can compute an integral sensitivity.

We compute the integral sensitivity as the flux of a source with a SED proportional to the SED of Crab Nebula giving $N_{\rm excess}/\sqrt{N_{\rm bkg}} = 5$ after 1 year, and integrating all energies above a given energy. The integral sensitivity is shown in Fig. 10.

5.8. Sensitivity to transient phenomena

To evaluate the capability of the detector to study sources with a fast luminosity variability in time, as well as to observe fast transient phenomena, we computed the integral sensitivity for a time window of one minute. Demanding a 3 sigma level above background we estimated a sensitivity of 25 Crab units above 100 GeV in one minute.

6. Prospects for the detection of transients

For their continuous on-time observations and their large effective area, extended arrays are ideal telescopes for transient phenomena. Among the transient sources whose study could greatly benefit from observation by particle arrays are: flares (mostly from AGN, occasionally from galactic sources like, as previously discussed, Crab Nebula); GRBs, whose few-seconds duration prompt emission has up to now precluded detection by ground-based gamma-ray instruments; possible electromagnetic counterparts of gravitational wave (GW) events. While

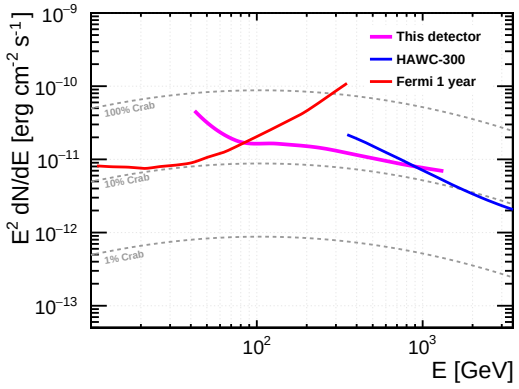

Figure 9: Differential sensitivity. We compute the flux of the source in a given energy range for which $N_{\rm excess}/\sqrt{N_{\rm bkg}} = 5$, $N_{\rm excess} > 10$, after 1 year of time (a 25% duty cycle has been assumed). 4 bins per decade in estimated energy are used. For comparison, fractions of the Crab Nebula spectrum are plotted with the thin dashed gray lines.

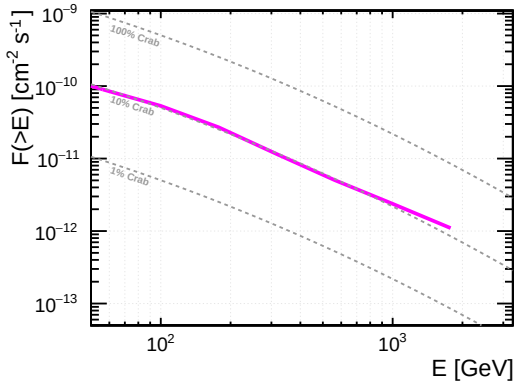

Figure 10: Integral sensitivity, defined as the flux of a source above a given energy for which $N_{\rm excess}/\sqrt{N_{\rm bkg}} = 5$ after 1 year; it is assumed that the SED is proportional to the SED of Crab Nebula. For comparison, fractions of the integral Crab Nebula spectrum are plotted with the thin, dashed, gray lines.

several flares from AGN have been recorded and the VHE spectrum has been often measured, there is large uncertainty in the VHE behavior of the SED from GRBs. Finally, the SED of EM counterparts of GW events, as well as the time delay and the duration, are still subject of speculations.

In the following we shall discuss the potential of the detector described in this article for the detection of flares and GRBs; we shall not discuss for the moment the potential for the detection of GW counterparts, since the information on the characteristics is too scarce.

6.1. Potential for the detection of flares

Most blazars undergo periods of strongly enhanced activity, associated to emission "flares" across the electromagnetic spectrum [see, e.g. 30]. These flares can boost the flux to tens or hundreds of times the baseline emission level. Not only the reason for the initiation and evolution of such flares is basically unknown, albeit probably originating by sudden increase in the infalling material rate, but also it is not always correlated along the electromagnetic spectrum. The relative weight of the flare changes from source to source and period to period. This is the most compelling reason to *a/* prepare multi-wavelengths campaigns on blazar targets to be triggered by one of the instruments in a network, and *b/* have a wide-FoV instrument, actually capable to trigger and observe for long time flaring episodes in the sky. Although a global account of flare durations and intensity in the VHE regime has not been compiled, it is known that flares can last from tens of seconds or few minutes (e.g., [31]) to several days.

In Fig. 11 we estimate the performance of the detector for flaring blazar targets. In black lines, we report the detector integral sensitivity accumulated in 1 day (5 standard deviations over the background), 1 hour, and 5 minutes (3 standard deviations over the background). These curves are obtained by rescaling the integral sensitivity plotted in Fig.10. We also report the Crab Nebula flux for reference. The figure also features three sets of points computed for hypothetical flares of 2.5, 5 and 7.5 Crab units (CU) considering a spectral photon index of -2, and calculated above 100, 500 and 1000 GeV.

Additionally, we overplot the fluxes from two real flares observed with IACTs:

Huge flare of Mrk 421 The blue diamonds show the huge flare observed with MAGIC and VERITAS on Markarian 421 in April 2013 [32]. The Astronomer Telegram states that the source was above 5 CU for several days, but very variable, and with a maximum of 20 CU, that is more than 20 times its baseline flux. This represented the highest level of VHE activity ever measured for that source although previous observations already reached the 10 CU level in 1996 [33] and 2010 [34]. This a prototype of strong and long-lasting flare: the source was extremely active for several days and the peak emission was registered after few days of observation. We assumed a rather standard spectral index of -2. We remark that besides the flux, also the spectral index can vary during the flare.

Faint flare of 1ES1011+496 A second real event is shown in green diamonds. This corresponds to the MAGIC observation of the flare of 1ES1011+496 in February 2014 [35]. In this case, the flare was seen for 6 days, and then faded away, with a peak of 1 CU on the 10th of February, in the 5th day of observation. The source emission could be fitted with a power law of spectral index −3, much softer than the Mrk421 one. This flare can be considered an usual flaring event, occurring several times per year in the VHE blazar catalogue.

The overlay of the fluxes from the flares and of the sensitivity lines cannot be interpreted straightforwardly. The sensitivity of the detector to blazar flare depends not only on the instantaneous and maximal intensity of the flare, but also on its duration, and its stability over time. Events like the Mrk421 flare are clearly observed with the detector described in this paper on a minute-time scale or even below across the full sensitive range. This would allow the detector to make a very dense inspection of the light curve over several hours in a day, and for the full period of activity of the source. As mentioned, not only this observable is very interesting per-se, potentially bearing important information, but also when put into a larger multi-wavelength context.

The detection of the 1ES1011+496 flare, representing a "faint" flare, requires instead more effort. From the figure, one can see that a significant detection can be accumulated only over one or few days of observation. While detection can therefore be guaranteed (as long as the flare duration lasts for more than few days), a significant measurement on the light curve would probably be less easily achievable, considering that the detector could only provide averages over daily activity.

The two above mentioned flares bracket the possibilities of the detector for the detection of blazar flares; a thorough check of the observability of the full sample of flares from current VHE instruments, considering flux variations, spectral indices evolutions, and flare duration, can in principle be done to estimate the average number of flares detectable by the detector over an year. Such a study is beyond the purpose of this paper.

6.2. Potential for the detection of GRBs

Based on the performance characteristics of the detector described here, we estimate the expected detection rate and sensitivity to GRB observations. With a reach of about 40° in zenith angle, and a corresponding FoV of about 2 sr, comparable to space-based instruments such as the *Fermi*-LAT, EAS arrays can serendipitously trigger on the prompt emission, rather than following it from external alerts.

In order to evaluate the detector's potential we simulated a set of 10 000 long-duration GRB events, which compose the bulk of LAT-detected GRBs. We do not consider short GRBs because of their low detection rate by *Fermi*-LAT and consequently uncertain high-energy spectral properties. All events are seen in identical, near zenith, observational conditions, following the same redshift distribution as revealed by the Gamma-ray Burst Monitor (GBM) onboard the *Fermi* satellite (see Fig. 19 in [36]). The baseline spectral model for the prompt emission follows the case of GRB090926A as a template [37], composed of a Band function to which we add a delayed, extended high-energy power law component with an intrinsic cut-off [38].

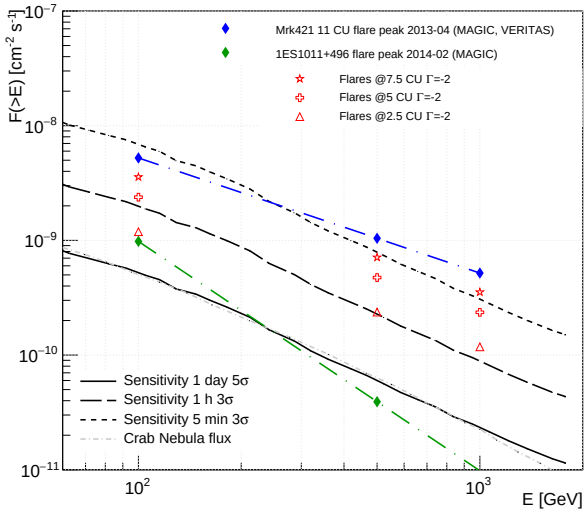
Mrk421 11 CU flare peak 2013-04 (MAGIC, VERITAS)
1ES1011+496 flare peak 2014-02 (MAGIC)
Flares @7.5 CU Γ=-2
Flares @5 CU Γ=-2
Flares @2.5 CU Γ=-2
Sensitivity 1 day 5σ
Sensitivity 1 h 3σ
Sensitivity 5 min 3σ
Crab Nebula flux
F(>E) [cm^{-2} s^{-1}]
E [GeV]

Figure 11: Performance of the detector proposed in this paper to benchmark blazar flares. Black lines show the detector integral sensitivity for 1 day (solid, 5σ), for 1 hour (long dashed, 3σ) and for 5 minutes (short dashed, 3σ), obtained by rescaling the sensitivity curve of Fig. 10. The Crab Nebula flux is also shown in light gray for reference. Three sets of points show hypothetical flares of 2.5, 5 and 7.5 Crab units (CU) (red empty triangles, crosses, stars respectively), considering a spectral photon index of −2, and calculated above 100, 500 and 1000 GeV. Additionally, two real flares observed by MAGIC and VERITAS are shown with blue diamonds (Mrk421 flare, April 2013, maximum emission around 11 CU, assumed spectral index −2) and green diamonds (1ES1011+496 flare, February 2014, maximum emission around 1 CU, spectral index −3. More details in the text.

The existence of this extended high-energy power-law spectral component was revealed by *Fermi*-LAT, and is responsible for the bulk of the GeV emission from GRBs. The choice of the cut-off at 100 GeV is somewhat arbitrary, as there is large uncertainty in the nature of the power-law component, but has been considered by other authors as a good approximation [39]. Spectral cut-offs below 100 GeV can significantly affect the detection rates presented here. Conversely, it is worth noticing that even in the absence of an intrinsic spectral cut-off, the detection of higher energy photons is strongly affected by EBL suppression above ∼ 100 GeV, given the cosmological distance of the sources. Our analysis is binned in three broad bands, corresponding to $z < 1$, $1 < z < 2$, and $z > 2$, and the EBL model adopted is that by [40], and is consistent with [41].

While spectral characteristics are fixed as shown in Fig. 12, the timing and flux properties were randomly sampled from a population with a range of parameters such as catalogued by *Fermi*-LAT [36]. The GeV extended emission was simulated as ranging from (10-600) s in duration, similar to the LAT T90 distribution > 100 MeV, after which the flux follows the typical extended emission phase decay of $t^{-1.5}$. The duration of the simulated GRB event is 10 times the value of T90, by when the extended high-energy signal has long decayed beyond detectability. We introduce a random delay to the onset of the

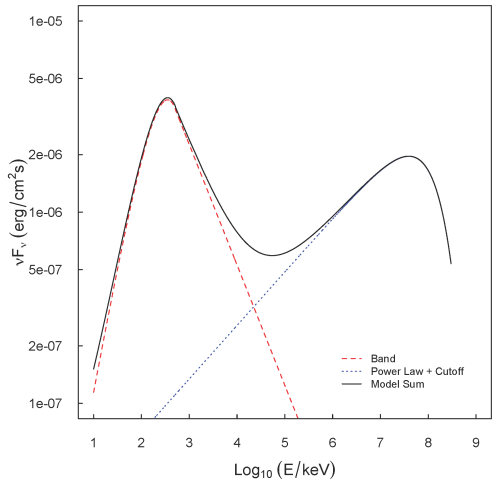

Figure 12: Template long GRB spectral model adopted in the Monte Carlo simulations. The plot shows the superposition of the prompt-emission Band function model with the extended high-energy power-law, with an intrinsic spectral cut-off at 100 GeV.

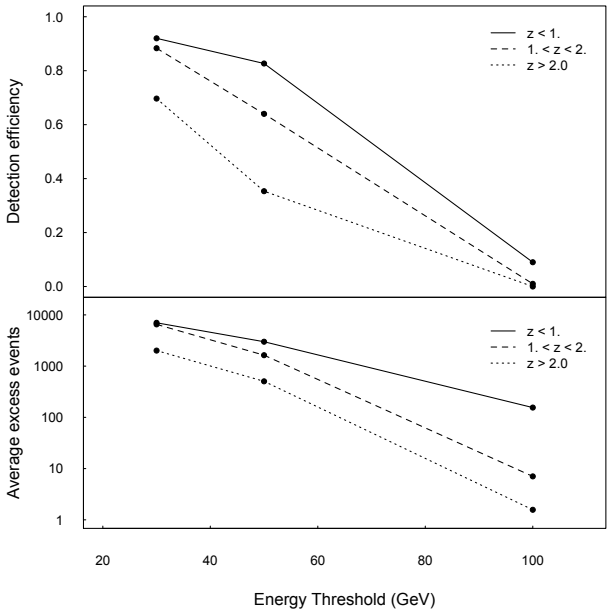

Figure 13: Top: detection efficiency (normalized) for 10 000 simulated GRBs as described in the text, as a function of the energy threshold of the observatory. Bottom: average number of gamma-ray photons collected above threshold for detected GRBs. The results are binned in redshift to emphasize the reach of the instrument.

high-energy power-law component with respect to the onset of prompt emission, which ranges typically from 4 s to 10 s. The fluence of the prompt emission phase is drawn from the typical range observed for LAT bursts, varying between 10^{-6} and 10^{-4} erg/cm^2 in the LAT energy sensitivity range. The fluence for the high-energy extended power-law is assumed to scale in the same way in order to keep a fixed fluence ratio between both components, as in [39]. The artificial GRB lightcurves were generated according to [42] following a typical power density spectrum (PSD) with index of -1.4 and threshold frequency of 1 Hz [43].

The simulation was performed in a photon-by-photon basis, each event having a time and an energy tag randomly assigned according to the description above. Due to the high fluence and short duration of GRBs, we are operating in a signal-dominated regime. We adopt a simplified approach by which a $\sigma_{\theta,68}$ cut is applied both to the signal and the background, corresponding to the effective area cuts in Fig. 5. As done for the Crab in the previous section, a source detection is considered positive only when a significance larger than 5 standard deviations was reached. Finally, the background is assumed as in Fig. 8 and roughly corresponds to 250 particles s^{-1} above 100 GeV, within the signal region, for a detector effective area of 10^4 m^2.

The top plot of Fig. 13 shows the detection efficiency of GRBs based on the criteria outlined above, for different detector energy thresholds. Here, detection efficiency is defined as the ratio between positive detections and total number of GRBs simulated. The signal integration was performed within a window containing 90% of the gamma-ray photons above threshold (T90) and not the entire duration of the simulated event, in order to maximize the signal-to-noise ratio. Distant sources remain challenging to observe due to strong EBL absorption above a few tens of GeV.

Data in the plots are binned in redshift; except in the case of a very low instrumental energy threshold, we do not expect to detect GRB events above $z = 2$. Despite the stringent constraints on the energy threshold, the number of photons observed from each detected GRB event is several orders of magnitude above what is seen by *Fermi*-LAT, as shown in the bottom plot of Fig. 13, meaning an unprecedented potential for detailed spectral and timing studies. In any case, it is necessary to bear in mind the large uncertainties involved in the GRB spectral model at high-energies.

Finally, what is the yearly rate of GRBs expected from the considerations above? Since an EAS array does not depend on external triggers, we can start our estimates from the about 200 long GRB per year detection rate from *Fermi* GBM [44], which has a FoV of about 8 sr, in comparison to the $\sim$ 2 sr of our instrument. Considering a nearly 100% operational duty cycle, and assuming a redshift distribution as mentioned above, we recover the estimates presented in Table 2.

E_{th}	30 GeV	50 GeV	100 GeV
Events	37	15	3

Table 2: GRB yearly detection rates expected for the baseline configuration with high-energy power-law cut-off at 100 GeV, and a detector effective area of 10^4 m^2. Event rates and redshift distribution are as referenced in the text.

Notice that even for a more conservative energy threshold of

100 GeV, we still expect a few GRB detections, corresponding to nearby events, closer than $z = 1$, for which several tens to a few hundred photons are expected to be recorded. For comparison, the current *Fermi*-LAT yearly detection rate is of 10 GRBs, with no more than a few dozen photons above 1 GeV collected for the brightest events. The numbers presented here are preliminary, but serve as a fiducial estimate for the potential of the observatory.

7. Summary

We have proposed a novel, large field-of-view, hybrid, extensive air shower detector sensitive to gamma rays of energies starting from 100 GeV (or even less for special high fluence transients), based on individual units made (from top to bottom) by:

- a thin slab of lead, to allow conversion of secondary photons in showers into electron-positron pairs;
- a position-sensitive detector like a RPC;
- a water Cherenkov detector (or any other electromagnetic calorimeter with some muon identification capabilities).

We have shown that such a detector, if deployed on a surface of some 10 000 m^2, can reach a sensitivity that can provide the missing link between the sensitivity of *Fermi* and the sensitivity of HAWC between 100 and 350 GeV, allowing to detect with a 5σ significance a source as faint as 10% of the Crab Nebula in one year, and able to survey half of the sky. The instrument can detect a source with the luminosity of 25 Crab at 3σ in 1 minute, making it a very powerful tool to trigger observations of variable sources, in particular flares by active galactic nuclei, and to detect transients coupled to gravitational waves and gamma-ray bursts.

The sensitivity of such a detector (expressed as minimum flux which can be detected at a given significance for a given time) scales approximately as $1/\sqrt{A}$, where A is the instrumented area.

An external sparse array of units would improve the angular resolution and the sensitivity at energies above the TeV. This fact would make such a detector a candidate for a possible new EAS gamma detector in the Southern hemisphere, complementary to the planned Cherenkov Telescope Array.

Acknowledgements

The authors thank B. De Lotto for her comments on the manuscript.

P. Assis and R. Conceição thank FCT-Portugal for the grants SFRH/BPD/102031/2014 and SFRH/BPD/73270/2010, respectively.

References

[1] A. De Angelis, M. Pimenta, *Introduction to particle and astroparticle physics* (Springer, 2015)
[2] B. Degrange, G. Fontaine, Comptes Rendus Physique **16**, 587 (2015)
[3] S. Funk, ArXiv e-prints (2015), 1508.05190
[4] A.M. Hillas, Astropart. Phys. **43**, 19 (2013)
[5] F. Acero, et al. (Fermi-LAT), ArXiv e-prints (2015), 1501.02003v3
[6] M. Ackermann, et al. (Fermi-LAT), Astrophys. J. **222**, 5 (2016)
[7] A.U. Abeysekara, et al. (HAWC), Astrophys. J. **817**, 3 (2016)
[8] L. Fuhrmann, et al., MNRAS **441**, 1899 (2014)
[9] F. Aharonian, et al. (HESS), Nature **531**, 476 (2016)
[10] A. Loeb, Astrophys. J. **819**, L21 (2016), 1602.04735
[11] W.B. Atwood, et al., Astrophys. J. **697**, 1071 (2009)
[12] J. Pretz, (for HAWC), in *Proceedings, 34th International Cosmic Ray Conference* (2015)
[13] A.U. Abeysekara, (for HAWC), in *Proceedings, 34th International Cosmic Ray Conference* (2015)
[14] G. Di Sciascio, (for LHAASO), in *Cosmic Ray International Seminar: The status and the future of the UHE Cosmic Ray Physics in the post LHC era (CRIS 2015)* (2016)
[15] M. Amenomori, et al. (Tibet-ASγ), Adv. Space Res. **47**, 629 (2011)
[16] B. Bartoli et al. (ARGO-YBJ), Astrophys. J. **779**, 27 (2013)
[17] A.M. Hillas, in *19th ICRC (La Jolla), Vol 3, 445* (1985)
[18] P. Abreu, (for AUGER), in *Proceedings, 34th International Cosmic Ray Conference* (2015)
[19] D. Heck et al., FZKA-6019 (1998)
[20] A. Ferrari et al., CERN-2005-010, SLAC-R-773, INFN-TC-05-11 (2005)
[21] T. Bŏhlen et al., Nuclear Data Sheets **120**, 211 (2014)
[22] S. Ostapchenko, Phys. Rev. **D83**, 014018 (2011)
[23] S. Agostinelli et al., Nucl. Instrum. Meth. **A506**, 250 (2003)
[24] J. Allison, et al., IEEE Trans.Nucl.Sci. **53**, 270 (2006)
[25] T.C. Weekes et al., Astrophys. J. **342**, 379 (1989)
[26] A.A. Abdo et al., Science **331**, 739 (2011)
[27] M. Tavani et al., Science **331**, 736 (2011)
[28] J. Aleksić et al. (MAGIC), JHEAp **5-6**, 30 (2014)
[29] A.U. Abeysekara, et al. (HAWC), Astropart. Phys. **50-52**, 26 (2013)
[30] K. Nalewajko, MNRAS **430**, 1324 (2013), 1211.0274
[31] J. Aleksic et al., Science **346**, 1080 (2014), 1412.4936
[32] J. Cortina, J. Holder, *MAGIC and VERITAS detect an unprecedented flaring activity from Mrk 421 in very high energy gamma-rays*, http://www.astronomerstelegram.org/?read=4976 (2013)
[33] J.A. Gaidos et al., Nature **383**, 319 (1996)
[34] L. Fortson (Fermi-LAT, VERITAS), AIP Conf. Proc. **1505**, 514 (2012)
[35] M.L. Ahnen et al., Astron. Astrophys. **590**, A24 (2016), 1602.05239
[36] M. Ackermann, et al. (Fermi-LAT), Astrophys. J. Suppl. Ser. **209**, 11 (2013)
[37] M. Ackermann, et al. (Fermi-LAT), Astrophys. J. **729**, 114 (2011)
[38] J. Kakuwa et al., MNRAS **425**, 514 (2012)
[39] R.C. Gilmore, et al. (CTA), Experimental Astronomy **35**, 413 (2013)
[40] R.C. Gilmore et al., MNRAS **422**, 3189 (2012)
[41] A. Franceschini, G. Rodighiero, M. Vaccari, Astron. Astrophys. **487**, 837 (2008)
[42] D. Emmanoulopoulos, I.M. McHardy, I.E. Papadakis, MNRAS **433**, 907 (2013)
[43] T.N. Ukwatta et al., MNRAS **412**, 875 (2011)
[44] S. Inoue et al. (CTA), Astropart. Phys. **43**, 252 (2013)